Odd−Even Effect in Molecular Packing of Biphenyl-Substituted Alkaneselenolate Self-Assembled Monolayers on Au(111): Scanning Tunneling Microscopy Study

Piotr Cyganik,*,† Katarzyna Szelagowska-Kunstman,† Andreas Terfort,‡ and Michael Zharnikov§

Research Centre for Nanometer-Scale Science and Advanced Materials (NANOSAM), Faculty of Physics, Astronomy, and Applied Computer Science, Jagiellonian University, Reymonta 4, 30-059 Kraków, Poland, Fachbereich Chemie, Universität Marburg, 35032 Marburg, Germany, and Angewandte Physikalische Chemie, Universität Heidelberg, 69120 Heidelberg, Germany

Received: June 16, 2008; Revised Manuscript Received: July 23, 2008

Self-assembled monolayers (SAMs) of hybrid ω-(4′-methylbiphenyl-4-yl) alkaneselenolates $CH_3(C_6H_4)_2(CH_2)_nSe$ (BPnSe, $n = 2-6$) on Au(111) substrates, prepared at room temperature, were studied using scanning tunneling microscopy. Molecularly resolved images reveal that all BPnSe species form well-ordered SAMs on Au(111), with rotational domains having typically a size of ca. 30−80 nm, which is about 5 times larger than their thiol analogues prepared at the same conditions. Two types of structures are alternatingly adopted depending on the parity of the number of the methylene units in the aliphatic linker of the BPnSe molecules. The unit cell of BPnSe SAMs with n = odd can be described as close to a commensurate oblique $(2\sqrt{3} \times \sqrt{3})R30°$ structure with two molecules per unit cell. The molecular arrangement in BPnSe SAMs with n = even can be described by anisotropic expansion of the above structure along its shorter unit cell vector. This expansion is, however, irregular so that the respective unit vector in this direction cannot be defined. As a result of this expansion, BPnSe SAMs with n = even are characterized by about 22−28% lower packing density than those with n = odd. For all systems, partial reorientation of the Au(111) step edges was observed upon SAM formation, indicating significant mobility of the topmost gold atoms induced by the adsorbates. The results for BPnSe/Au(111) systems are discussed in view of the previously reported spectroscopic data and compared with the analogous results for the BPnS/Au(111) films.

I. Introduction

Progress in molecular electronics relies upon the design of molecular devices combining desired electronic properties and ease of arrangement in micro- and nanostructures. Aromatic self-assembled monolayers (SAMs)[1] are a very promising prototype system to meet these demands, since these films offer both the control over their electronic functionality[2−10] and the potential to assemble molecular devices.[1,11−13] However, to fabricate aromatic SAMs of practical importance, a high level of control over the structure and properties of these systems should be achieved. Such control is, however, a difficult task, since the structure of a SAM is generally determined by a complex interplay of several factors, viz. the intermolecular interactions, molecule−substrate bonding, and lattice mismatch between the most favorable molecular lattice and the substrate.

An experimental approach to gain a general concept for the rational design of SAMs includes a systematic modification of the chemical composition of the SAM constituents and detailed investigation of the structure and properties of the resulting SAMs. Following this general idea in recent years, we investigated in depth a homologue series of thiol-based SAMs on Au(111) and Ag(111), the thermodynamically favored and thus technologically most important surfaces. The molecules, $CH_3(C_6H_4)_2(CH_2)_nSH$ (BPnS, $n = 1-6$), combine the biphenyl moiety and an aliphatic linker of variable length inserted between this moiety and the thiol headgroup, permitting us to determine the influence of both structural elements on the structure of the SAMs. A combination of detailed spectroscopic[14−16] and microscopic[17,18] investigations revealed that such a seemingly minor element as a short aliphatic linker has a fundamental influence on the molecular structure of the resulting SAMs, whose entire structure and packing density changes depending on either an odd or even number n of the methylene units in the linker. Moreover, it was shown that these systematic odd−even structural changes are accompanied by the respective variation of the film properties, including their electrochemical stability,[19,20] stability toward exchange by other molecules capable to build SAMs on the same substrate,[21] reaction to electron irradiation,[22] and existence of thermally induced irreversible phase transitions.[23−25] On the basis of these findings and, in particular, on the odd−even effect in thermally induced phase transitions,[23−25] we proposed a simple qualitative model[24] where the relation between the SAM structure and its stability is determined by either a cooperative or competitive way the different factors determining the energetics of a SAM enter into the energy balance. This has been illustrated (see Figure 11 in ref 24) by a model where the Au−S−C bending potential and the density of the S−Au bonds along with the intermolecular interactions are the key factors determining the energy of the system. While for BPnS SAMs on Au(111) with n = odd all these factors act cooperatively, the Au−S−C bending potential opposes the other two factors in the films with n = even. As a consequence, BPnS SAMs on Au(111) with n = even are less stable and may undergo phase transitions into new, more stable structures. The key element of this phenomenological

* Corresponding author. E-mail: piotr.cyganik@uj.edu.pl.
† Jagiellonian University.
‡ Universität Marburg.
§ Universität Heidelberg.

10.1021/jp805303r CCC: $40.75
Published on Web 09/09/2008

model is the significant contribution of the exact bonding configuration of the BPnS molecule on the surface (i.e., the Au−S−C bending potential) to the overall energetics of the BPnS film. The existence of such bending potential directly follows from the available spectroscopic data[15] which demonstrated that the odd−even changes in the packing and orientation of the BPnS molecules are reversed once the substrate is changed from Au(111) to Ag(111), and, thus, the preferable value of the substrate−S−C angle is changed from ∼104° to ∼180°, respectively.

As documented by the recent review by Tao and Bernasek,[26] there is not much theoretical work regarding odd−even effects in SAMs. This is probably related to the complexity of the problem requiring the exact consideration of the Au(111) substrate reconstruction and precise knowledge on the absorption site geometry, which is still under discussion even for such a simple system as methane thiolate on Au(111).[27−29] Note, however, that the available DFT calculations, even though performed with some simplified assumptions, reproduce the odd−even changes in the preferable conformation of the substrate−S−C bond in the BPn/Au(111) systems.[30]

To further test our quantitative model and thus get a better insight into the basic design rules of aromatic SAMs, one should consider modification of the headgroup. In this regard, selenium is a very promising candidate, since, as a higher homologue of sulfur in the 16th group of the periodic table, it has a similar valence electron configuration. Also, from the viewpoint of potential applications the choice of selenium seems to be well justified by recent investigations. Combined spectroscopic and microscopic studies performed by us clearly demonstrated that in the case of purely aromatic SAMs drastic improvement in the film structure quality can be achieved as a result of the substitution of S by Se, which makes Se a perspective alternative to S.[31] Note that this general conclusion was reproduced recently[32] by other purely aromatic SAMs that were used in our original study.[31] Along with this improvement, the electronic conductance of selenium-based aromatic molecules is predicted to be comparable[33] or even significantly higher[34−36] than that of their sulfur analogues. The latter prediction seems to be confirmed by a very recent ultraviolet photoelectron spectroscopy investigation of purely aromatic thiols and selenols on the Au(111) surface, indicating a smaller charge injection barrier for the gold−selenium as compared to that of the gold−sulfur interface.[37]

In view of the above arguments, we examine here the influence of the S → Se substitution on the microscopic structure of the biphenyl-substituted aliphatic SAMs on Au(111) substrate for the homologue series of $CH_3(C_6H_4)_2(CH_2)_nSe$ (BPnSe, n = 2−6) molecules. The results are discussed in light of the spectroscopic data reported by us recently for these systems,[38,39] as well as compared to the previously reported STM data for the corresponding thiol-based analogues (i.e., BPnS/Au(111)).[17] Note that our series does not include the BP1Se films, since they have a low quality, which is presumably related to an exceptional chemistry of the respective precursor on Au(111).[39]

II. Experimental Section

Sample Preparation. The precursor molecules for BPnSe SAM fabrication were diselenide compounds (BPnSe−SeBPn: $CH_3(C_6H_4)_2(CH_2)_nSe-Se(CH_2)_n(C_6H_4)_2CH_3$). The synthesis of these molecules was described elsewhere.[40] The gold films were prepared in a deposition chamber operated at a base pressure of $\sim 10^{-7}$ mbar by evaporating (rate 2 nm/s) 150 nm of gold onto mica substrates at 610 K. Before deposition, the freshly cleaved mica sheets had been heated at the evaporation temperature for about 24 h under vacuum conditions to remove residual water. After deposition, the gold/mica substrates were flame-annealed in a butane/oxygen flame. This procedure yielded high-quality gold films with flat terraces of several 100 nm exhibiting a (111) surface orientation and steps faceting along the $\langle 1\bar{1}0\rangle$ directions. The BPnSe SAMs were prepared by immersion of Au(111) substrates into a 0.1 mM solution of the respective BPn diselenide (BPnSe−SeBPn) in ethanol at room temperature for 24 h. After immersion, samples were rinsed with pure ethanol and blown dry with nitrogen.

Scanning Tunneling Microscopy (STM) Measurements. All STM measurements were carried out in air at room temperature using a MultiMode IIIa (Digital Instruments) instrument. In all cases, tips were prepared mechanically by cutting a 0.25-mm Pt/Ir alloy (8:2, Goodfellow) wire. The data were collected in constant current mode using tunneling currents in the range of 20−50 pA and a sample bias between 0.7 and 1.2 V (tip positive). No tip-induced changes were observed under these imaging conditions.

III. Results

The results are summarized in Figures 1−5 showing STM images and height profiles obtained for the BPnSe SAMs with n = odd (Figures 1 and 2) and n = even (Figures 3, 5). All figures were organized in a similar way, presenting STM images taken at different length scales to reveal (1) possible substrate changes and the domain boundary network at a large scale, (2) the structure inside domains with characteristic intermolecular distances at intermediate scale, and finally, (3) clear identification of all molecules within the observed structures at the highest resolution scale.

BPnSe SAMs with n = Odd. STM data obtained for the BP3Se SAM are presented in Figure 1. Even the images taken at large scale (shown in Figure 1a) bring two interesting observations. First, the step edges of the Au(111) substrate show partial change of their orientation from the $\langle 1\bar{1}0\rangle$ to $\langle 11\bar{2}\rangle$ directions, which results in formation of characteristic kinks not observed on the Au(111) substrate before the SAM formation. To facilitate identification of this rearrangement, all $\langle 1\bar{1}0\rangle$ and $\langle 11\bar{2}\rangle$ directions are indicated in Figure 1a. The second important observation is a clear STM contrast modulation in the form of stripes. This pattern is better visible at larger magnification, as shown in Figure 1b. Although these stripes do not represent perfectly straight lines and both the distance between them and their orientation are not perfectly regular, they adopt certain preferred orientations, forming clear domain structures. Interestingly, the relative orientation of these domains, as indicated by the red and yellow arrows in Figure 1b, does not show the threefold symmetry of the underlying Au(111) substrate. Generally, as indicated in Figure 1a, which shows a much larger area of the sample, these domains are oriented in six different directions (marked by the colored arrows). Moreover, these six directions can be grouped into two threefold groups (marked with either red or yellow arrows), which, as clearly indicated in Figure 1a by combining all directions together, correspond to directions being about ±12−16° off the closest high-symmetry substrate directions, which are the $\langle 11\bar{2}\rangle$ ones. The relative orientation of the stripe pattern and $\langle 11\bar{2}\rangle$ directions is more clearly documented in Figure 1c, which shows an angle β of about 45° (60−15°) between a line along the stripes and one of the $\langle 11\ \bar{2}\rangle$ substrate directions. High-resolution data presented in Figure 1d,e show that this stripe pattern does not correspond to any visible domain boundaries network but

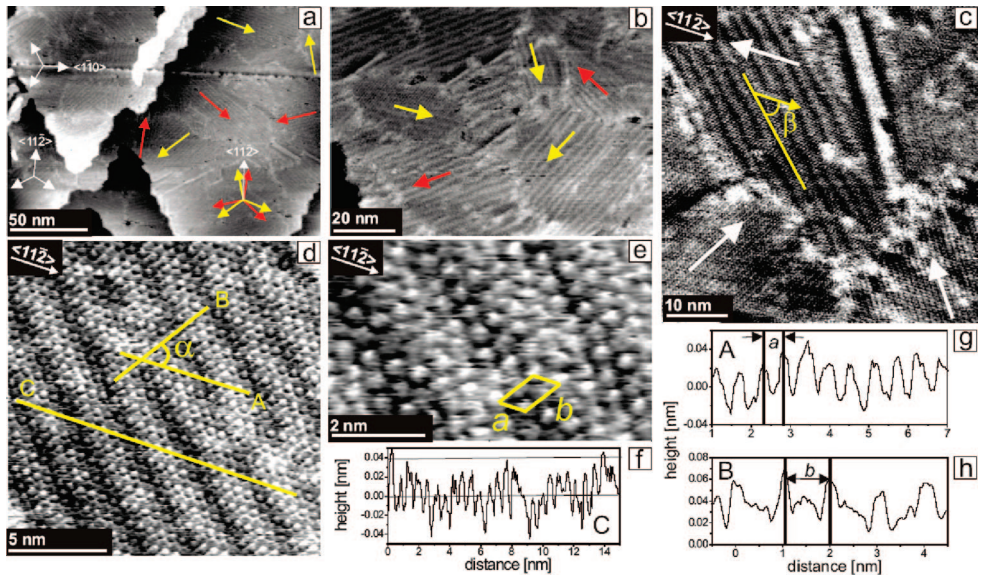

Figure 1. STM data for BP3Se SAMs on Au(111). (a−e) STM images taken with different resolutions and (f−h) height profiles C, A, and B, taken along the lines depicted in (d). (a, b) Yellow and red arrows show six possible directions of domains formed by stripe pattern (see text for details). (c) Angle $\beta \approx 45°$ marks relative orientation of the stripe pattern lines (see text for details) and one of the $\langle 11\bar{2} \rangle$ substrate directions. White arrows mark the orientation of three different rotational domains following the $\langle 11\bar{2} \rangle$ directions. (e) The oblique box marks the $(2\sqrt{3} \times \sqrt{3})$R30° unit cell with the *a* and *b* dimensions marked in the height profiles presented in (g) and (h), respectively.

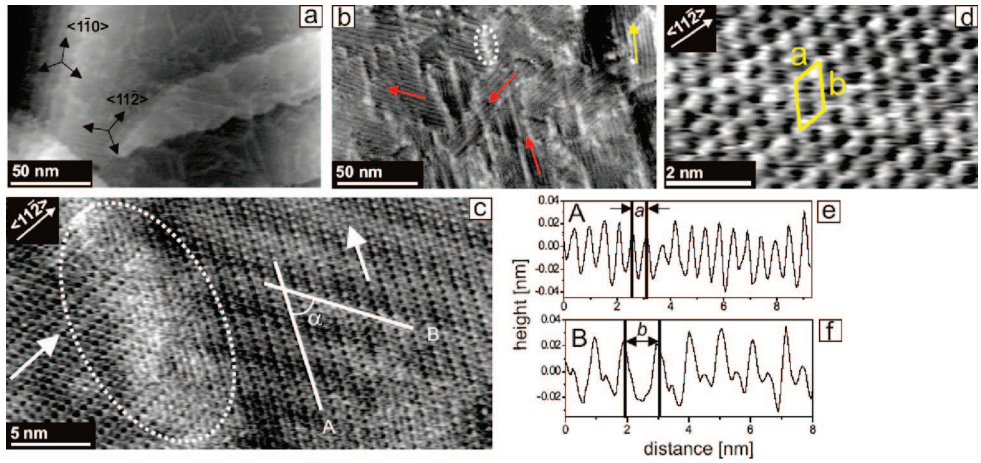

Figure 2. STM data for BP5Se SAMs on Au(111). (a−d) STM images taken with different resolutions and (e, f) height profiles A and B, taken along the lines depicted in (c). (b) Yellow and red arrows show four out of generally six directions of domains formed by the stripe pattern (see text for details). The white dotted loop marks one of the domain boundary regions. (c) White arrows mark orientation of two out of three possible different rotational domains following the $\langle 11\bar{2} \rangle$ directions. The white dotted loop marks one of the domain boundary regions. (d) The oblique box marks the $(2\sqrt{3} \times \sqrt{3})$R30° unit cell with *a* and *b* dimensions marked in the height profiles presented in (e) and (f), respectively.

appears only as an additional contrast modulation overimposed on the molecular lattice. As indicated by the cross section C taken from the STM image in Figure 1d and presented in Figure 1f, the contrast modulation related to the observed stripe pattern corresponds to about 0.03−0.04-nm difference in height. The molecular structure of the BP3Se film is characterized by the molecular rows along the $\langle 11\bar{2} \rangle$ substrate directions, showing alternating contrast variation every second row. The orientation of these rows follows the threefold symmetry of the Au(111) substrate, and only three rotational domains were observed, as indicated by white arrows in Figure 1c. The structure can be described by an oblique unit cell (indicated in Figure 1e) containing two molecules. The dimensions of this unit cell (*a* and *b* in Figure 1d) as well as its orientation relative to the Au(111) template can be measured using height profiles A and B from the STM image in Figure 1d (Figure 1g,h). The analysis performed for five different STM images revealed average values of $a = 0.53 \pm 0.03$ nm, $b = 1.30 \pm 0.05$ nm, and an angle $\alpha = 61 \pm 3°$.

Data obtained for the BP5Se SAM are presented in Figure 2. The results are very similar to those for the BP3Se film. The large-scale image in Figure 2a shows the same kinks formation on the step edges, indicating their partial reorientation from the $\langle 1\bar{1}0 \rangle$ to the $\langle 11\bar{2} \rangle$ direction. Also in this case, a stripe pattern formation was observed, with the orientation of the individual domains showing generally the same six different directions (Figure 2b with the arrows pointing to four out of six different directions) as described in details above for the BP3Se system. The observed stripe pattern can not be associated with any visible domain boundaries of the molecular structure (Figure 2c). High-resolution STM images presented in Figure 2c,d confirm formation of a densely packed structure with an oblique unit cell containing two molecules. Within the error limits, this structure has the same dimensions and orientation relative to

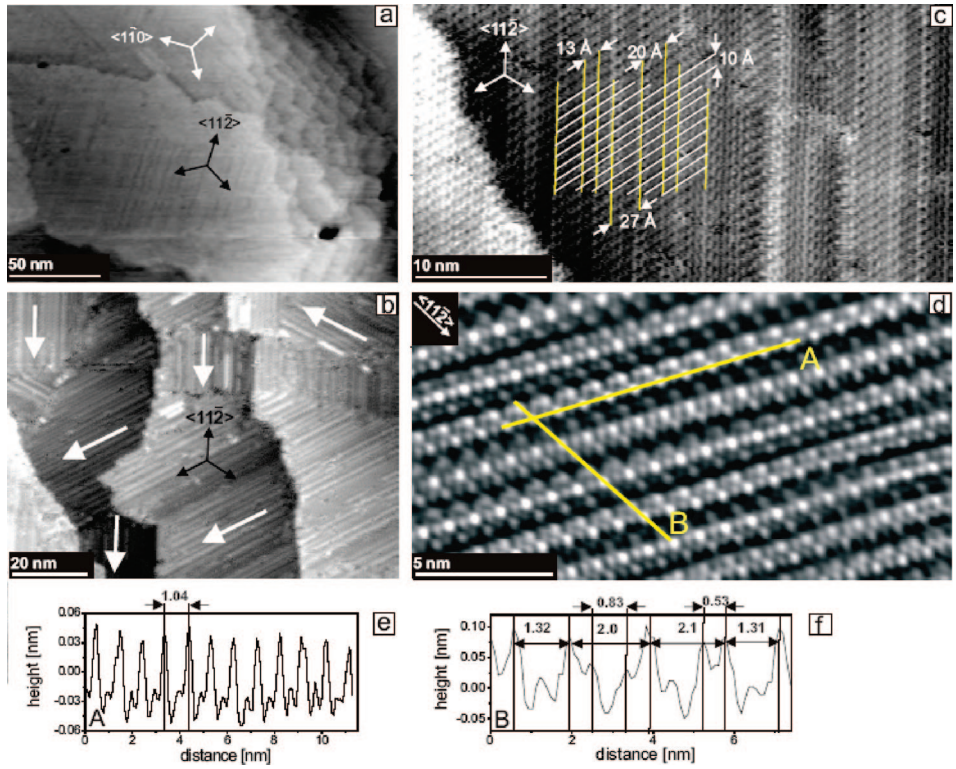

Figure 3. STM data for BP2Se SAMs on Au(111). (a−d) STM images taken with different resolutions and (e, f) height profiles A and B, taken along the lines depicted in (d) (see text for details). (b) White arrows show three directions of domains formed by stripe pattern following exactly the ⟨11$\bar{2}$⟩ directions (see text for details). (c) A single rotational domain is shown with white lines marking regularly spaced rows of molecules following the ⟨11$\bar{2}$⟩ directions, and yellow lines marking irregular spaced stripes crossing these rows at 60° (i.e., along another ⟨11$\bar{2}$⟩ equivalent direction).

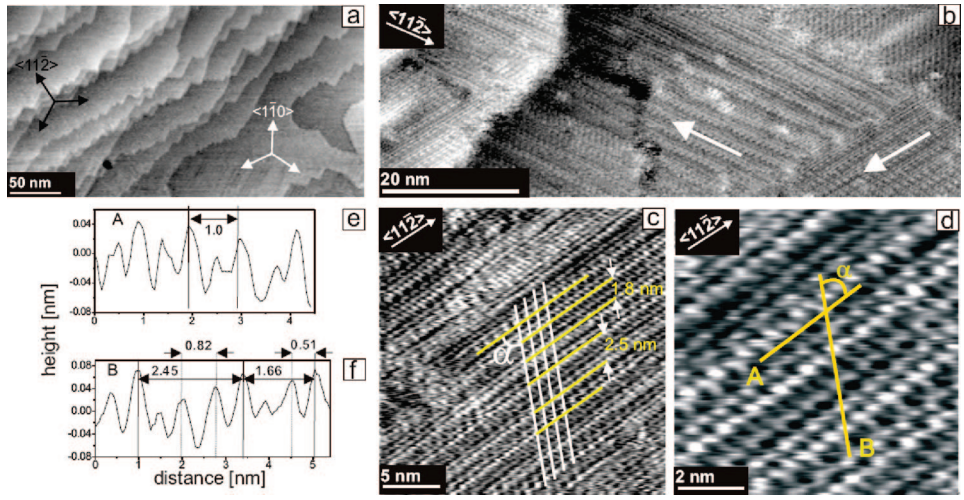

Figure 4. STM data for BP4Se SAMs on Au(111) substrate. (a−d) STM images taken with different resolutions and (e, f) height profiles A and B, taken along the lines depicted in (d) (see text for details). (b) White arrows show two out of three different directions of domains formed by stripe pattern following exactly the ⟨11$\bar{2}$⟩ directions (see text for details). (c) A single rotational domain is shown with white lines marking regularly spaced rows of molecules following the ⟨11$\bar{2}$⟩ directions and yellow lines marking irregular stripes crossing these rows at α = 60° (i.e., along another ⟨11$\bar{2}$⟩ equivalent direction).

the substrate as was reported for the BP3Se systems, that is, the average values for *a*, *b*, and α are 0.51 ± 0.03 nm, 1.02 ± 0.04 nm, and 59 ± 3°, respectively (height profiles A and B marked in Figure 2c and presented in Figure 2e,f).

For both BP3Se and BP5Se, domain boundaries visible in Figures 1b and 2b are characterized by local increase in the STM measured height. The apparent width of the domain boundaries at this scale is about 5−8 nm, which can be associated with some major structural defects or contaminations located at these boundaries (dotted loop in Figure 2b). However, a high-resolution image of the rotational domain boundary shows that the molecular structure within these regions remains mainly unchanged and that the real width of the domain boundary is about 1 nm (Figure 2c, see the area indicated by the dotted loop).

BPnSe SAMs with *n* = Even. STM data for the BP2Se monolayer are summarized in Figure 3. Images taken at large scale (Figure 3a) reveal kinks formation at the step edges, showing the same reorientation of the these edges as was observed for the BPnSe SAMs with *n* = odd. Images taken at

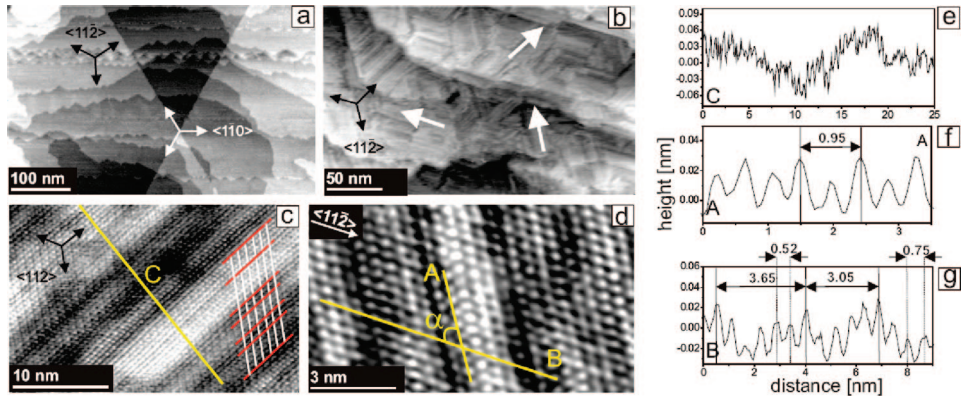

Figure 5. STM data for BP6Se SAMs on Au(111). (a−d) STM images taken with different resolutions and (e−g) height profiles A, B, and C taken along the lines depicted in (d) and (c), respectively (see text for details). (b) White arrows show three different directions of domains formed by stripe pattern following exactly the $\langle 11\bar{2}\rangle$ directions (see text for details). (c) A single rotational domain is shown with white lines marking regularly spaced rows of molecules following the $\langle 11\bar{2}\rangle$ directions, and red lines marking irregularly spaced stripes crossing these rows at $\alpha = 60°$ (i.e., along another $\langle 11\bar{2}\rangle$ equivalent direction).

intermediate scale exhibit stripe pattern formation, which is, however, completely different from what was reported for the SAMs with n = odd. First, the domains are oriented along three directions only, being perfectly aligned with the $\langle 11\bar{2}\rangle$ substrate directions (Figure 3b). Second, the spacing between the stripes, their width, and relative contrast modulation are very irregular within a single rotational domain. Figure 3c presenting a molecular resolution STM image of BP2Se/Au(111) shows that this irregular stripe pattern is combined with the molecular rows running along another equivalent $\langle 11\bar{2}\rangle$ direction (i.e., at the angle of 60° with respect to the stripes), showing alternating contrast every second row. As indicated in Figure 3c, the distance between the alternating molecular rows measured along the direction of the stripe pattern is very regular and corresponds to about 1.0 nm. In contrast, the distance between the stripes measured across the direction of the alternating molecular rows is irregular (e.g., 1.3, 2.0, or 2.7 nm), as marked in Figure 3c. More detailed analysis of this structure is presented in Figure 3d, and the height profiles A and B taken from this image are shown in Figure 3e,f, respectively. Whereas the distance between the molecules along height profile A (i.e., along the stripe pattern) is regular and, on the average (taken from five different images), corresponds to about 0.51 ± 0.03 nm, the distance between the molecules across the direction of the stripe pattern varies between 0.52 and 0.84 nm, as indicated in Figure 3f. This distance variation is fully correlated with the stripe structure. The average value of the intermolecular spacing, measured across a few stripes, amounts to about 0.64 ± 0.04 nm.

For the BP4Se SAMs, very similar data was collected, with representative results presented in Figure 4. The restructuring of the step edges and the resulting kinks formation are well visible in Figure 4a. Also in this case, the stripe pattern perfectly follows the substrate $\langle 11\bar{2}\rangle$ directions (Figure 4b), and its width is irregular as exemplified in Figure 4c. Figure 4c,d reveals the same molecular structure as for the BP2Se system, that is, the molecular packing in the form of alternating rows (marked by yellow lines in Figure 4c) following one of the $\langle 11\bar{2}\rangle$ directions and the stripe pattern intersecting this structure at an angle (α) of about 60° (i.e., along another $\langle 11\bar{2}\rangle$ equivalent direction). The height profiles A and B taken from the STM image presented in Figure 4d and depicted in Figure 4e,f, respectively, show that, within the error bars, the distances between the molecules along the height profiles A and B are the same as those for the BP2Se film (i.e., 0.50 ± 0.03 and 0.61 ± 0.04 nm, respectively). Again, as was commented on in more detail for BP2Se, the intermolecular spacing along the height profile B for BP4Se film can only be defined as an average value, since it varies (between 0.50 and 0.82 nm) in coincidence with the stripe pattern (see the distances marked in Figure 4f).

Figure 5 shows a summary of the STM data obtained for the BP6Se SAMs. Similar to the two other BPnSe SAMs with n = even, we also observed in this case partial reorientation of the step edges (Figure 5a) and formation of the strip pattern (Figure 5b) strictly following the substrate symmetry. However, STM images presented in Figure 5c show that this stripe pattern appears not only at a short scale (1−3 nm) as for BP2Se and BP4Se, but also at a larger scale of about 20−40 nm. Whereas the former observation is consistent with the results for the two other BPnSe SAMs with n = even (Figures 3c and 4c), the latter was only observed for the BP6Se SAMs. The height profile C taken from the STM image presented in Figure 5c and depicted in Figure 5e shows that the STM contrast variation related to the long-range stripe pattern corresponds to about 0.1 nm, which is 2−3 times larger than the height variation related to the short-range stripe pattern clearly visible at higher resolution (see the height profile B in Figure 5g). However, apart from both short- and long-range contrast variation, the molecular structure of the BP6Se SAMs, as exemplified by the data presented in Figure 5c,d, is, within the precision of our STM measurements, fully consistent with the structure obtained for the two other BPnSe SAMs with n = even as described above. The intermolecular distances measured along the height profiles A and B correspond to about 0.51 ± 0.03 and 0.62 ± 0.04 nm, respectively, with the latter value being an average across several stripes because of its variation (between 0.50 and 0.82 nm; see the data in Figure 5g) as was commented for the BP2Se and BP4Se SAMs.

IV. Discussion

We start the discussion with the observations that are common for all the systems of this study. The first feature shared by all these systems is the appearance of kinks on the substrate step edges upon SAM formation. This feature is a consequence of partial reorientation of the step edges from the $\langle 1\bar{1}0\rangle$ directions known as energetically preferred on the Au(111) substrate[41] to the $\langle 11\bar{2}\rangle$ ones. A similar effect was also observed by us previously for the BP0Se SAMs on Au(111), which was prepared at the same conditions.[31] Interestingly, such a reori-

entation of the substrate step edges was not observed for the respective thiol-based SAMs (BPnS/Au(111), $n = 0-6$) despite the same preparation procedure.[17,42] For the BP4S and BP6S SAMs, partial reorientation of the step edges was only observed in parallel with the structural phase transitions, but only after a long (15−24 h) annealing of the SAMs at relatively high temperature (423 K) in air.[24] This indicates that the mobility of the gold atoms in the topmost layer of the substrate increases significantly upon the substitution of S for Se in the biphenyl-based SAMs. It is well-known that metal−metal bonds in the surface layer can be weakened by the chemisorbed adsorbates, leading to an increased mobility of the surface metal atoms.[43,44] For the SAMs on the metal substrate, the activation energy for the gold atom mobility should depend on the strength of the metal−molecule bond, adsorbate coverage, and intermolecular interactions in the SAMs. Since both surface coverage and the intermolecular interactions in the BPnSe and BPnS SAMs are very similar (see discussion below), the strength of the metal−molecule bond is the most decisive factor. In view of this conclusion, the observed differences in the temperature behavior of BPnSe/Au and BPnS/Au suggest that the Au−Se bond is somewhat stronger then the Au−S one, in agreement with conclusions reached by most of the authors on the basis of spectroscopic and electrochemical data for aliphatic[45−47] and aromatic[48] thiolates and selenolates. An opposite conclusion was reached only in the first publications on selenolate SAM by Samant et al.[49] and in a recent study by Witte et al.[32] However, in the work by Samant et al., this conclusion was only a speculation and was not supported by any concrete experimental data. The conclusion by Witte et al. is also questionable in our opinion, since the interpretation of the thermal desorption spectroscopy data is not unambiguous and can be turned the other way around.

The second feature common to all BPnSe films is the formation of significantly larger domains as compared to the respective thiol-derived SAMs. For the BPnSe SAMs, domains with a characteristic diameter of about 30−80 nm are formed even at room temperature, whereas only 5−20-nm domains are observed at the same preparation conditions in the BPnS SAMs. In the latter system, only a temperature increase to 343 K allows the formation of domains of size comparable to that for BPnSe.[17] Since the structures of the BPnSe and BPnS SAMs are very similar, one can only conclude that the higher mobility of BPnSe molecules on the Au(111) surface is associated with the change in the molecule−substrate energetics. The assumption of the slightly stronger Au−Se bond as compared to the Au−S one is not at variance with such a higher mobility. It is well-known that it is not the strength of the molecule−substrate bond but the lateral corrugation of the headgroup−substrate potential hypersurface that defines the mobility of the SAM constituents with respect to the template lattice provided by the substrate.[51] In view of this statement, our STM data clearly indicate a lower lateral corrugation of the headgroup−substrate potential for BPnSe/Au(111) as compared to that of BPnS/Au(111).

Considering details of the molecular structure for the individual systems, we start with discussion of the BPnSe SAMs with n = odd. The STM images obtained for the BP3Se and BP5Se SAMs are very similar. The change in the STM contrast in every second molecular row along the $\langle 11\bar{2} \rangle$ directions can be ascribed to the herringbone arrangements of the phenyl backbones, which is characteristic of the structure of biphenyl single crystals[52] and was concluded for most of the aromatic SAMs.[17,18,23,50,53−55] Within the STM precision, both distances between the molecules and adsorbate lattice orientation with

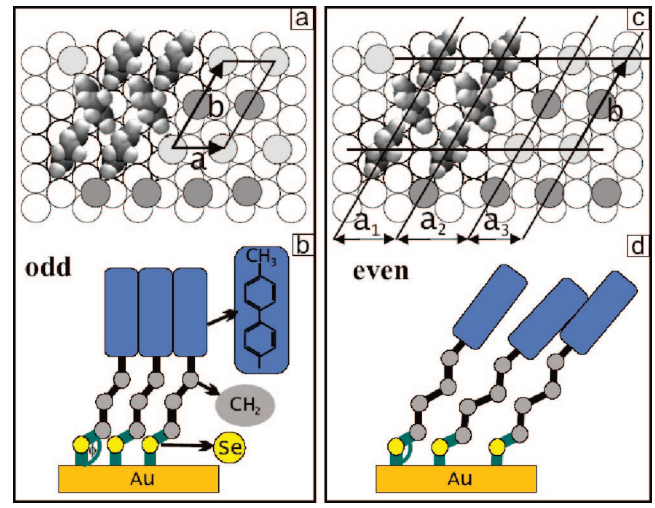

Figure 6. Schematic illustration of the structure of the BPnSe SAMs on Au(111) with n = odd (a, b) and n = even (c, d). (a, c) Schematic top views of the structures. Open circles correspond to gold atoms on the Au(111) surface; light and dark gray filled circles correspond to Se atoms with adsorption sites taken arbitrary. (a) The $(2\sqrt{3} \times \sqrt{3})R30°$ unit cell is marked, with the a and b basis vectors and the herringbone arrangement of phenyl rings. (b) The $(2\sqrt{3} \times \sqrt{3})R30°$ unit cell is irregularly expanded toward the direction of vector a (which is schematically shown by different values of a: $a_1 \approx 0.63$, $a_2 \approx 0.73$, and $a_3 \approx 0.53$ nm) with phenyl rings following herringbone arrangement. (b, d) Schematic side views of the structures, indicating the tilting of the biphenyl moieties (not included in (a) and (b) for a sake of clarity), which is larger and probably more inhomogeneous for BPnSe/Au(111) SAMs with n = even.

respect to the substrate would suggest a commensurate $(2\sqrt{3} \times \sqrt{3})R30°$ structure with two molecules per unit cell and an area per molecule of 0.216 nm^2, as schematically shown in Figure 6a. The same structure was reported by us previously for BPnS/Au(111) with n = 3 and 5. However, for BPnSe/Au(111) systems with n = odd, this molecular lattice coexists with an additional stripe pattern, as revealed by STM, whose orientation does not strictly follow the symmetry of the substrate. This indicates that a $(2\sqrt{3} \times \sqrt{3})R30°$ lattice commensurate with the Au(111) substrate has to be considered only as an approximation of a generally not fully commensurate lattice. Importantly, this stripe structure does not disturb the molecular lattice as measured by the STM. A similar phenomenon was observed by us previously for the SAMs of the thiol analogues (BPnS), but only after a prolonged annealing.[56] We attribute this additional pattern to the domain boundaries (solitons) at the molecule−substrate interface. As proposed previously,[56] formation of such domains is a form of stress relaxation in hybrid aliphatic−aromatic SAMs. This stress originates from the misfit between the structure preferred by the aromatic moieties and the structural template provided by the substrate. For rigid, purely aromatic SAMs such a misfit results in a dense network of domain boundaries affecting aromatic structure, whereas in more flexible hybrid aliphatic−aromatic systems the presence of the aliphatic linker gives the possibility to leave aromatic structure to a large extent unaffected and relax stress by a combination of factors involving conformational degrees of freedom of the spacer and deviations of the sulfur lattice from a perfect commensurate structure.[56] However, it should be noted at this point that despite its higher flexibility in comparison to the aromatic part of the molecule, the aliphatic linker is still "rigid" enough to transfer orientation of the Au−Se−C bond to the biphenyl part of the molecule and thus enable the observed odd−even effect in the film structure. Note

that since STM probes the SAM structure at the top of the aromatic moiety, the changes taking place at the molecule−substrate interface, and not affecting the structure of the aromatic part of the film, will only affect STM contrast but not the distances measured between the molecules.

The STM data obtained for the films with $n = 2$, 4, and 6 suggest that all BPnSe SAMs with $n =$ even have a similar structure. Similar to the films with $n =$ odd, the change in the STM contrast in every second molecular row along the $\langle 11\bar{2}\rangle$ directions can be ascribed to the herringbone arrangements of the biphenyl moieties (Figure 6b). Both the threefold orientation of these rows, forming rotational domains, and the distance between them (ca. 0.87 nm) are the same as those for BPnSe SAMs with $n =$ odd. However, in contrast to the latter films, the distance between the molecules along these rows is irregular and on average about 22−28% larger. Moreover, no systematic lattice constant could be found along these rows resulting in formation of an irregular network of stripes intersecting the alternating rows of molecules at a fixed angle of ca. 60° (Figure 6b). Thus, the structure of the BPnSe SAMs with $n =$ even can be described as an anisotropic expansion of the $(2\sqrt{3} \times \sqrt{3})$R30° lattice typical for the films with $n =$ odd along its shorter unit cell vector (vector a in Figure 6a). This expansion is, however, irregular, so that the unit vector in this direction cannot be defined. As a result of this expansion, the structure of the BPnSe SAMs with $n =$ even is characterized by 22−28% lower packing density, which corresponds to an area per molecule of about 0.260−0.275 nm^2. Also for the thiol analogues of these films, the structure can be described as a similar expansion of the $(2\sqrt{3} \times \sqrt{3})$R30° lattice in exactly the same direction that leads, however, to the formation of the regular rectangular $(5\sqrt{3} \times 3)$ structure with an area per molecule of about 0.270 nm^2 (α-phase)[17,24] (i.e., close to the value observed for the respective BPnSe SAMs). Note that the perfect orientation of the irregularly spaced stripes intersecting the alternating molecular rows at 60° indicates that BPnSe films with $n =$ even are energetically close to a structure with an oblique unit cell. Interestingly, a similar commensurate oblique structure, even though with lower packing density (0.324 nm^2/molecule), was observed for BP4S/Au(111) and BP6S/Au(111) after the preparation at elevated temperature or post annealing (β-phase).[24]

The appearance of the additional long-range contrast modulation for the BP6Se film (height profile C in Figure 5b,c) in contrast to the BP2Se and BP4Se SAMs indicates that not only the odd or even number of the CH_2 units in the aliphatic linker of the BPnSe molecule but also the length of this linker influences the detailed structure of the BPnSe−Au interface and, thus, the way in which relaxation of the stress is realized. It is not surprising, since apart from the changing intermolecular interactions, an increased length of the aliphatic chain gives more freedom for the molecular arrangement.

In closing, we would like to refer to our recent spectroscopic results.[38,39] As shown in the present study, BPnSe SAMs with $n =$ odd are characterized by the structure close to commensurate $(2\sqrt{3} \times \sqrt{3})$R30° lattice, whereas this lattice is expanded along one of the $\langle 11\bar{2}\rangle$ directions in the films with $n =$ even, which results in comparably lower packing density of the latter layers. This observation is fully consistent with high-resolution X-ray photoelectron spectroscopy (HRXPS), near-edge X-ray absorption fine structure spectroscopy, ellipsometry, and infrared spectroscopy data, which suggest lower packing density and larger molecular inclination for the BPnSe SAMs with $n =$ even. Furthermore, the analysis of the HRXPS spectra demonstrated a systematically larger width of the Se $3d_{5/2,3/2}$ peaks for the films with $n =$ odd (see Figure 3 in ref 39) and thus indicated a more diverse distribution of the adsorption sites for the Se headgroups on the Au(111) substrate. On first sight, this conclusion seems to be at variance with the STM results presented here, which clearly show that BPnSe SAMs with $n =$ odd are better ordered. However, as was discussed above, the $(2\sqrt{3} \times \sqrt{3})$R30° lattice has to be considered only as an approximation of a generally noncommensurate structure formed by $n =$ odd BPn systems. Otherwise, one could not explain the existence of the domain boundaries structure at the BPnSe−Au interface, which is presumably responsible for the appearance of the additional stripe contrast in the STM images observed for BPnSe SAMs with $n =$ odd.

V. Conclusions

The STM results presented here demonstrated pronounced dependence of the molecular packing and crystallographic structure of the BPnSe/Au(111) SAMs on the parity of the number (n) of the CH_2 units in the aliphatic linker of the BPnSe molecules. For $n =$ odd, densely packed structure with an area per molecule of about 0.216 nm^2 was observed, which is close to commensurate $(2\sqrt{3} \times \sqrt{3})$R30° lattice. In contrast, for $n =$ even, this lattice is uniaxially expanded along one of the $\langle 11\bar{2}\rangle$ directions with undefined periodicity along the direction of expansion. The resulting structure is characterized by a noticeable lower packing density (an area per molecule of about 0.260−0.275 nm^2) than that for $n =$ odd. The observed odd−even variation of the packing density is fully consistent with previous spectroscopic measurements performed on the same systems.[39] This effect can be explained by the directional character of the Au−Se−C bond, which is an important factor entering the interplay of structure−building interaction in alkaneselenolate SAMs. The preferable orientation given by this bond is transferred to the biphenyl moiety by the aliphatic linker, which is obviously sufficiently rigid to fulfill this function, and whose parity becomes the decisive parameter for the orientation and, consequently, the packing density of the biphenyl moieties.

The odd−even effects characteristic of the BPnSe SAMs were previously observed in the BPnS films as well, which allows us to proclaim the generality of these effects for aliphatic SAMs with chalcogen headgroups. Considering the differences between BPnSe and BPnS SAMs on Au(111) substrate, we noted the reorientation of Au(111) substrate step edges upon adsorption of BPnSe molecules, which indicates higher adsorbate-induced mobility of the gold atoms in the top layer and, thus, somewhat stronger bonding to the substrate in comparison to their thiol analogues (BPnS). The other distinctive feature of the BPnSe SAMs is the quite large size of the crystalline domains, which typically are ca. 30−80 nm, about 5 times larger than their thiol analogues prepared at the same conditions. We relate this feature to a smaller corrugation of the binding energy hypersurface for Se−Au(111) as compared to that of S−Au(111).

Whereas in the case of BPnS SAMs well-defined crystallographic structures (with odd−even varying different packing density) were observed for both $n =$ odd and $n =$ even,[17,18] the molecular arrangements, which we found in BPnSe SAMs with $n =$ even, are, strictly speaking, not crystallographic lattices, since there is no fixed periodicity along one of the basic directions. Thus, the difference between the structures with $n =$ odd and $n =$ even is more pronounced for BPnSe SAMs as compared to their thiol analogues.

Acknowledgment. We thank Professor Marek Szymonski for providing the access to the STM microscope at the Department

of Physics of Nanostructures and Nanotechnology at Jagiellonian University. The work was supported by the Polish Ministry of Science and Higher Education (0061/B/H03/2008/34). P.C. greatly acknowledges the *Homing* fellowship from the Foundation for Polish Science and Maria Curie Host Fellowship (MTKD-CT-2004-003132). M.Z. thanks M. Grunze for the support and acknowledges the funding by DFG (ZH 63/10-1).

References and Notes

(1) Love, J. C.; Estroff, L. A.; Kriebel, J. K.; Nuzzo, R. G.; Whitesides, G. M. *Chem. Rev.* **2005**, *105*, 1103–1170.
(2) Beebe, J. M.; Kushmerick, J. G. *Appl. Phys. Lett.* **2007**, *90*, 083117.
(3) Venkataraman, L.; Klare, J. E.; Nuckolls, C.; Hybertsen, M. S.; Steigerwald, M. L. *Nature* **2006**, *442*, 904–907.
(4) Tran, E.; Duati, M.; Ferri, V.; Mullen, K.; Zharnikov, M.; Whitesides, G. M.; Rampi, M. A. *Adv. Mater.* **2006**, *18*, 1323–1328.
(5) Boyen, H.-G.; Ziemann, P.; Wiedwald, U.; Ivanova, V.; Kolb, D. M.; Sakong, S.; Gross, A.; Romanyuk, A.; Buttner, M.; Oelhafen, P. *Nat. Mater.* **2006**, *5*, 394–399.
(6) Katsonis, N.; Kudernac, T.; Walko, M.; Molen, S. J.; Wees, B. J.; Feringa, B. L. *Adv. Mater.* **2006**, *18*, 1397–1400.
(7) Seminario, J. M. *Nat. Mater.* **2005**, *4*, 111–113.
(8) Flood, A. H.; Stoddart, J. F.; Steuerman, D. W.; Heath, J. R. *Science* **2004**, *306*, 2055–2056.
(9) Fan, F. R. F.; Lai, R. Y.; Cornil, J.; Karzazi, Y.; Bredas, J.; Cai, L. T.; Cheng, L.; Yao, Y.; Price, D. W.; Dirk, S. M.; Tour, J. M.; Bard, A. J. *J. Am. Chem. Soc.* **2004**, *126*, 2568–2573.
(10) Li, C.; Zhang, D. H.; Liu, X. L.; Han, S.; Tang, T.; Zhou, C. W.; Fan, W.; Koehne, J.; Han, J.; Meyyappan, M.; Rawlett, A. M.; Price, D. W.; Tour, J. M. *Appl. Phys. Lett.* **2003**, *82*, 645–647.
(11) Smith, R. K.; Lewis, P. A.; Weiss, P. S. *Prog. Surf. Sci.* **2004**, *75*, 1–68.
(12) Felgenhauer, T.; Yan, C.; Geyer, W.; Rong, H. T.; Gölzhäuser, A.; Buck, M. *Appl. Phys. Lett.* **2001**, *79*, 3323–3325.
(13) Thom, I.; Hähner, G.; Buck, M. *Appl. Phys. Lett.* **2005**, *87*, 024101–024103.
(14) Zharnikov, M.; Frey, S.; Rong, H.; Yang, Y. J.; Heister, K.; Buck, M.; Grunze, M. *Phys. Chem. Chem. Phys.* **2000**, *2*, 3359–3362.
(15) Rong, H. T.; Frey, S.; Yang, Y. J.; Zharnikov, M.; Buck, M.; Wühn, M.; Wöll, C.; Helmchen, G. *Langmuir* **2001**, *17*, 1582–1593.
(16) Heister, K.; Rong, H. T.; Buck, M.; Zharnikov, M.; Grunze, M.; Johansson, L. S. O. *J. Phys. Chem. B* **2001**, *105*, 6888–6894.
(17) Cyganik, P.; Buck, M.; Azzam, W.; Wöll, C. *J. Phys. Chem. B* **2004**, *108*, 4989–4969.
(18) Azzam, W.; Cyganik, P.; Witte, G.; Buck, M.; Wöll, C. *Langmuir* **2003**, *19*, 8262–8270.
(19) Thom, I.; Buck, M. *Surf. Sci.* **2005**, *581*, 33–46.
(20) Long, Y. T.; Rong, H. T.; Buck, M.; Grunze, M. *J. Electroanal. Chem.* **2002**, *524*, 62–67.
(21) Felgenhauer, T.; Rong, H. T.; Buck, M. *J. Electroanal. Chem.* **2003**, *550*, 309–319.
(22) Frey, S.; Rong, H. T.; Heister, K.; Yang, Y. J.; Buck, M.; Zharnikov, M. *Langmuir* **2002**, *18*, 3142–3150.
(23) Cyganik, P.; Buck, M.; Strunskus, T.; Shaporenko, A.; Witte, G.; Zharnikov, M.; Wöll, C. *J. Phys. Chem. C* **2007**, *111*, 16909–16919.
(24) Cyganik, P.; Buck, M.; Strunskus, T.; Shaporenko, A.; Wilton-Ely, J. D. E. T.; Zharnikov, M.; Wöll, C. *J. Am. Chem. Sci.* **2006**, *128*, 13868–13878.
(25) Cyganik, P.; Buck, M. *J. Am. Chem. Soc.* **2004**, *126*, 5960–5961.
(26) Tao, F.; Bernasek, S. L. *Chem. Rev.* **2007**, *107*, 1408–1453.
(27) Kondoh, H.; Iwasaki, M.; Shimada, T.; Amemiya, K.; Yokoyama, T.; Ohta, T.; Shimomura, M.; Kono, S. *Phys. Rev. Lett.* **2003**, *90*, 066102.
(28) Maksymovych, P.; Sorescu, D. C.; Yates, J. T. *Phys. Rev. Lett.* **2006**, *97*, 146103.
(29) Mazzarello, R.; Cossaro, A.; Verdini, A.; Rousseau, R.; Casalis, L.; Danisman, M. F.; Floreano, L.; Scandolo, S.; Morgante, A.; Scoles, G. *Phys. Rev. Lett.* **2007**, *98*, 0161021.
(30) Heimel, G.; Romaner, L.; Bredas, J.; Zojer, E. *Langmuir* **2008**, *24*, 474–482.
(31) Shaporenko, A.; Cyganik, P.; Buck, M.; Terfort, A.; Zharnikov, M. *J. Phys. Chem. B* **2005**, *109*, 13630–13638.
(32) Bashir, A.; Käfer, D.; Müller, J.; Wöll, C.; Terfort, A.; Witte, G. *Angew. Chem., Int. Ed.* **2008**, *47*, 5250–5253.
(33) Heimel, G.; Romaner, L.; Zojer, E.; Bredas, J. *Nano Lett.* **2007**, *7*, 932–940.
(34) Di Ventra, M.; Lang, N. D.; Pantelides, S. T. *Chem. Phys.* **2002**, *281*, 189–198.
(35) Di Ventra, M.; Lang, N. D. *Phys. Rev. B* **2001**, *65*, 045402.
(36) Yaliraki, S. N.; Kemp, M.; Ratner, M. *J. Am. Chem. Soc.* **1999**, *121*, 3428–3434.
(37) Yokuta, K.; Taniguchi, M.; Kawai, T. *J. Am. Chem. Soc.* **2007**, *129*, 5818–5819.
(38) Shaporenko, A.; Müller, J.; Weidner, T.; Terfort, A.; Zharnikov, M. *J. Am. Chem. Soc.* **2007**, *129*, 2232–2233.
(39) Weidner, T.; Shaporenko, A.; Müller, J.; Schmid, T.; Cyganik, P.; Terfort, A.; Zharnikov, M. *J. Phys. Chem. C* **2008**, *112*, 12495–12506.
(40) Müller, J.; Terfort, A. *Inorg. Chim. Acta* **2006**, *359*, 4821–4827.
(41) Li, Y. G.; DePristo, A. E. *Surf. Sci.* **1996**, *351*, 189–199.
(42) Azzam, W.; Fuxen, C.; Birkner, A.; Rong, H. T.; Buck, M.; Wöll, C. *Langmuir* **2003**, *19*, 4958–4968.
(43) Sette, F.; Hashizume, T.; Comin, F.; MacDowell, A. A.; Citrin, P. H. *Phys. Rev. Lett.* **1988**, *61*, 1384–1387.
(44) Trevor, D. J.; Chidsey, C. E. D.; Loiacono, D. N. *Phys. Rev. Lett.* **1989**, *62*, 926–932.
(45) Shaporenko, A.; Ulman, A.; Terfort, A.; Zharnikov, M. *J. Phys. Chem. B* **2005**, *109*, 3898–3906.
(46) Yee, C. K.; Ulman, A.; Ruiz, J. D.; Parikh, A.; White, H.; Rafailovich, M. *Langmuir* **2003**, *19*, 9450–9458.
(47) Sato, Y.; Mizutani, F. *Phys. Chem. Chem. Phys.* **2004**, *6*, 1328–1331.
(48) Weidner, T.; Shaporenko, A.; Müller, J.; Höltig, M.; Terfort, A.; Zharnikov, M. *J. Phys. Chem. C* **2007**, 11627–11635.
(49) Samant, M. G.; Brown, C. A.; Gordon, J. G., II. *Langmuir* **1992**, *8*, 1615–1618.
(50) Käfer, D.; Bashir, A.; Witte, G. *J. Phys. Chem. C* **2007**, *111*, 10546–10551.
(51) Ulman, A. *Chem. Rev.* **1996**, *96*, 1533–1554.
(52) Trotter, J. *Acta Crystallogr.* **1961**, *14*, 1135–1140.
(53) Käfer, D.; Witte, G.; Cyganik, P.; Terfort, A.; Wöll, C. *J. Am. Chem. Soc.* **2006**, *128*, 1723–1732.
(54) Kang, J. F.; Ulman, A.; Liao, S.; Jordan, R.; Yang, G. H.; Liu, G. Y. *Langmuir* **2001**, *17*, 95–106.
(55) Yang, G. H.; Qian, Y. L.; Engtrakul, C.; Sita, L. R.; Liu, G. Y. *J. Phys. Chem. B* **2000**, *104*, 9059–9062.
(56) Cyganik, P.; Buck, M.; Wilton-Ely, J. D.; Wöll, C. *J. Phys. Chem. B* **2005**, *109*, 10902–10908.

JP805303R